Critical behavior of ferromagnetic perovskite ruthenates

J.-G. Cheng,[1] J.-S. Zhou,[1,*] J. B. Goodenough,[1] and C.-Q. Jin[2]

[1]*The Materials Science Program/Mechanical Engineering, University of Texas at Austin, Austin, Texas 78712, USA*

[2]*Institute of Physics, Chinese Academy of Science, Beijing 100080, China*

(Received 18 November 2011; revised manuscript received 19 April 2012; published 29 May 2012)

Stoner-Wohlfarth itinerant-electron ferromagnetism has been believed to be applicable to the metallic, ferromagnetic perovskite $SrRuO_3$. A key piece of evidence is the linearity of the Arrott plot M^2 versus H/M obtained in a previous study. However, a typical Heisenberg behavior observed in isostructural $BaRuO_3$ raises a question how the small structural change between them can place these compounds into two extremes of magnetic interactions. For clarification of this issue, we carried out magnetization measurements in the vicinity of T_c for the whole series of ferromagnetic ruthenates from $Ca_{0.5}Sr_{0.5}RuO_3$ to $SrRuO_3$ to $BaRuO_3$. Moreover, we studied the effects of the A-site size variance and hydrostatic versus nonhydrostatic pressure on the Arrott plot of $SrRuO_3$. Our results reveal that the magnetization behavior as presented by the Arrott plot is extremely sensitive to structural distortions. The linearity of the Arrott plot for $SrRuO_3$ is actually part of a continuous curvature evolution as lattice distortions and spin-orbit coupling change; it may have little to do with Stoner-Wohlfarth itinerant-electron ferromagnetism. The data for these ruthenates point to a distinct phase appearing between localized-electron and broad-band behavior that exhibits a strong ferromagnetism stabilized by strong correlations among electrons of a narrow band.

DOI: 10.1103/PhysRevB.85.184430 PACS number(s): 75.30.−m, 75.40.−s, 75.10.Lp, 75.30.Et

I. INTRODUCTION

Ferromagnetism has been described for two limiting cases by Stoner-Wohlfarth itinerant-electron magnetism in metals and Heisenberg magnetism in either metals or insulators. The mean-field theory works well to describe magnetic properties in paramagnetic and magnetically ordered phases except in the vicinity of a magnetic transition where critical fluctuations become severe, especially for Heisenberg magnets. Exponents in the power law to describe critical fluctuations can be extracted from the Arrott plot[1] of the magnetization $M(H)$ near T_c. Very weak itinerant-electron ferromagnetism[2] always shows parallel isothermal lines in the plot of M^2 versus H/M for both paramagnetic and ferromagnetically ordered phases whereas Heisenberg ferromagnetism[3] exhibits curved isotherms with a uniform concave curvature, as illustrated in Fig. 1 for temperatures on crossing T_c. In the case of Heisenberg ferromagnetism, the linearity can be restored in a more general plot of $M^{1/\beta}$ versus $(H/M)^{1/\gamma}$ with $\beta < 0.5$ and $\gamma > 1$. Exponents can be further refined through iterations between the power-law fitting in $M_s(T)$, $\chi_0(T)$ obtained in Fig. 1 and the modified Arrott plot with exponents from the power-law fitting. The self-consistent renormalization (SCR) model[4,5] has been put forward to account for ferromagnetism in metallic systems where the electron-electron correlations are too strong for Stoner-Wohlfarth itinerant-electron ferromagnetism. The latest development of this model by Takahashi[6] can account explicitly for a deviation from lines to curves with a slightly concave curvature in an Arrott plot depending on the ratio of $\eta = T_c/T_0$, where T_c is the Curie temperature and T_0 is the characteristic temperature of spin fluctuations, which can be derived directly from neutron inelastic scattering or an NMR measurement. Linearity in the Arrott plot M^2 versus H/M is obtained for a ferromagnet with small η, as in $ZrZn_2$ having $\eta = 0.053$, for instance. The SCR model[6] has been applied successfully to explain the anomalous ferromagnetism in MnSi ($\eta \approx 0.13$), which shows curves with a slightly concave curvature in an Arrott plot. However, it is a challenge to apply the SCR model to explain the nearly linear parallel lines of the Arrott plot found in the $M(H)$ of the perovskite $SrRuO_3$[7] in which η is at least as large[8] as that of MnSi. The linearity of the Arrott plot and a large η appear contradictory to each other on the basis of current models. On the other hand, the close relationship between metallic conductivity and ferromagnetism found in the ultrathin-film samples of $SrRuO_3$ seems to support the model of itinerant-electron ferromagnetism.[9] As reported recently,[10] the cubic $BaRuO_3$, which has essentially the same physical properties as that of $SrRuO_3$, exhibits in the Arrott plot isotherms with a uniform concave curvature typical of a Heisenberg ferromagnet. A much reduced T_c and the complete suppression of T_c under $P = 8$ GPa in the cubic $BaRuO_3$ indicate that the cubic $BaRuO_3$ has a much broader bandwidth than that in $SrRuO_3$. The bandwidth consideration is clearly not compatible with the argument of Stoner-Wohlfarth itinerant-electron ferromagnetism in $SrRuO_3$ and Heisenberg ferromagnetism in $BaRuO_3$. In order to clarify this issue, we have carried out a systematic study of the magnetization in the vicinity of T_c for all ferromagnetic members in the perovskite family of $ARuO_3$ with $A = Ca_{1-x}Sr_x$, $Sr_{1-y}Ba_y$. We have also found that the critical behavior is extremely sensitive to lattice strains and local disorder due to either the size variance effect and nonhydrostatic component if high pressure is applied. We have argued that the strong ferromagnetism of the $ARuO_3$ perovskites is a distinguishable phase appearing at a crossover from Pauli paramagnetism to localized-electron behavior in a $4d$ band where spin-orbit coupling is progressively enhanced as the bandwidth narrows. The interplay between spin-spin interactions and the strong spin-orbit coupling invalidates the classic criterion for itinerant-electron ferromagnetism, viz. the linearity of the Arrott plot.

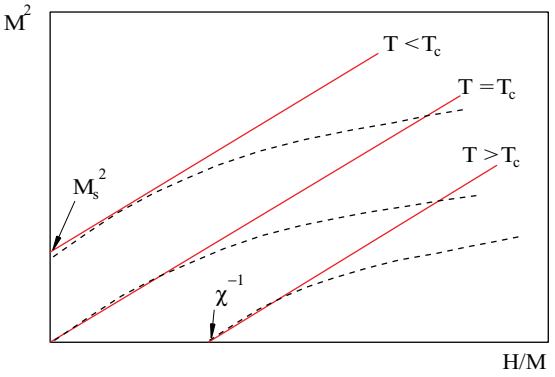

FIG. 1. (Color online) Schematic of the Arrott plot of magnetization for ferromagnets in two extreme limits. Solid lines can be predicted by the equation of state $M^2 = M_0{}^2[1 - (T/T_c)^2 + 2\chi_0 H/M]$, which is applicable for a very weak, itinerant-electron ferromagnet. At $T > T_c$, isotherms intercept the H/M axis at the inverse susceptibility χ^{-1}, whereas they intercept the M^2 axis at the spontaneous magnetization $M_s{}^2$ at $T < T_c$. Curves of dashed lines with a concave curvature are typical for ferromagnets described by Heisenberg, XY, and Ising models.

II. EXPERIMENTAL METHODS

All samples in this study were made with starting materials ACO_3 (A = Ca, Sr, Ba) and Ru or RuO_2. The well-mixed starting materials were sintered at temperatures 800–1100 °C in air with several intermediate grindings. This procedure produced a single phase with the orthorhombic *Pbnm* perovskite structure for all compositions of $Sr_{1-y}Ca_yRuO_3$ ($0 \leqslant y \leqslant 1$), but produced hexagonal polytypes (i.e. 4H, 6H, 9R) or mixed phases depending on x for the compositions of $Sr_{1-x}Ba_xRuO_3$ ($0 < x \leqslant 1$). While keeping the average A-cation size $\langle r_A \rangle$ constant, a size variance $\sigma^2 = \langle r_A^2 \rangle - \langle r_A \rangle^2$ was introduced into these samples by substituting $(Ba_{0.49}Ca_{0.51})$ for Sr. For example, $\langle r_A \rangle$ remains the same while σ^2 increases gradually with increasing z in the series $Sr_{1-z}(Ba_{0.49}Ca_{0.51})_zRuO_3$. Because the effective ionic radii of Ca^{2+}, Sr^{2+}, and Ba^{2+} depend sensitively on their coordination number, which decreases from XII for cubic $BaRuO_3$ to VIII for highly distorted orthorhombic $CaRuO_3$, we have chosen the effective ionic radius of Ca^{2+}(VIII): 1.12 Å, Sr^{2+}(X): 1.36 Å, and Ba^{2+} (XII): 1.61 Å for calculation of $\langle r_A \rangle$ and σ^2 in the present study. For those compositions containing Ba, high-pressure and high-temperature synthesis under 3–18 GPa and 1000 °C is required in order to obtain a single phase with perovskite structure; it was carried out in a Walker multianvil module (Rock and Research). The x-ray powder diffraction was performed with a Philips X'pert diffractometer and the Rietveld refinement on these diffraction spectra was made with FULLPROF. Magnetic properties of the ruthenates were measured in a superconducting quantum interference device (SQUID) magnetometer (Quantum Design). The pressure effect on the magnetization was carried out in a Be-Cu self-clamped cell fitting into a commercial SQUID magnetometer. As the pressure medium, we have used two kinds of fluids: 3M Fluorinert FC77 & FC72 and silicon oil. The sample's demagnetization factor is determined by the magnetization at low field. However, subtraction of the demagnetization field from the external field H_0 does not influence the output of the Arrott plot, so this correction has not been made in our plots.

III. RESULTS AND DISCUSSIONS

Since all compositions containing Ba need to be synthesized under high pressure and the high-pressure synthesis has an obvious influence on the magnetization even for samples in which the high-pressure synthesis is not necessary, we show in Fig. 2 the Arrott plots for high-pressure ferromagnetic products of all the ruthenate perovskites in order to demonstrate the A-cation size effect. We start from $A = Sr_{0.5}Ca_{0.5}$, which has the smallest average A-cation size $\langle r_A \rangle$ in this study. The feature inside the dashed circle around the origin in this Arrott plot will be discussed in the last paragraph of this section; we first focus on isotherms outside the circle.

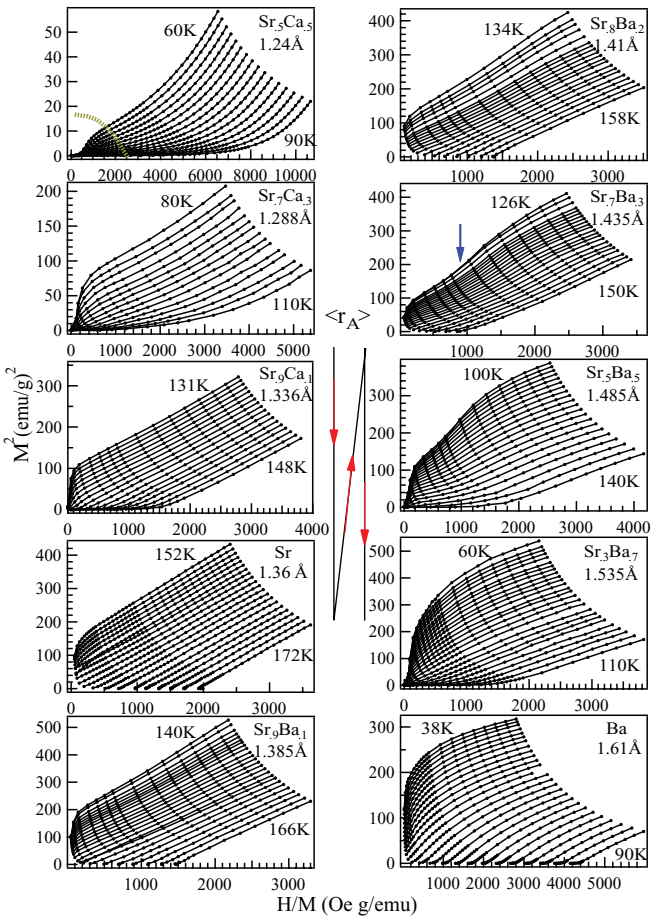

FIG. 2. (Color online) Arrott plots M^2 versus H/M for perovskites $ARuO_3$ (I. the effect of A-cation size). These plots are organized according to their average A-cation size $\langle r_A \rangle$ in the order shown by the diagram in the center of the figure. $BaRuO_3$ shows uniform curves with concave curvature on crossing T_c; the linearity is restored with a modified Arrott plot $M^{1/\beta}$ versus $(H/M)^{1/\gamma}$. An A-cation size variance distorts the plot so severely that the isothermal curves are no longer uniform on crossing T_c; the size variance creates a convex curvature in the curves below T_c as shown by the arrow in $A = Sr_{0.7}Ba_{0.3}$. The combination of the size variance and the structural distortion associated with a smaller $\langle r_A \rangle$ converts all curves to a convex curvature in the plot of $A = Sr_{.5}Ca_{.5}$.

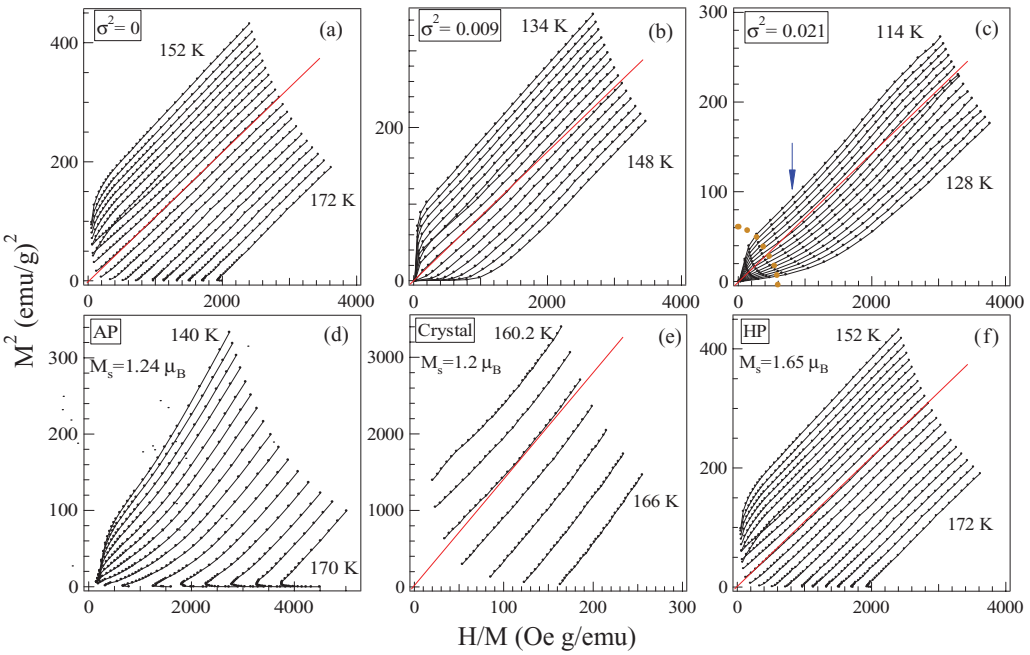

FIG. 3. (Color online) Arrott plots M^2 versus H/M for perovskites $ARuO_3$ (II. the effects of size variance and high-pressure treatment). (a)–(c) These three samples have an identical $\langle r_A \rangle = r_{Sr}$ but different σ^2 as labeled inside each panel. Lines are a guide to the eyes. The linearity deteriorates as σ^2 increases. The size variance clearly causes the convex curvature at low fields as identified in (c). (d)–(f) These three samples are the polycrystalline $SrRuO_3$ synthesized under ambient pressure (AP), single crystal $SrRuO_3$ (Crystal), whose plot is digitized from Ref. 7 (note that the unit of magnetization in this plot is emu/cm^3), and polycrystalline $SrRuO_3$ synthesized under 4 GPa and 1000 °C (HP).

As illustrated in Fig. 2, isotherms for temperatures on crossing T_c have a uniform convex curvature for the sample $Sr_{0.5}Ca_{0.5}RuO_3$; this behavior of the Arrott plot cannot be accounted for with existing models. The degree of convex curvature decreases gradually as $\langle r_A \rangle$ increases. Almost perfectly linear isotherms are found in the Arrott plot for $SrRuO_3$. As $\langle r_A \rangle$ increases further by substituting Ba for Sr, isotherms in the Arrott plot are no longer uniform and the curvature changes at different values of H/M. Since isotherms with uniform concave curvature are found in $BaRuO_3$, which has the largest $\langle r_A \rangle$, it is reasonable to attribute a concave curvature at higher H/M to the effect due to enlarging $\langle r_A \rangle$. On the other hand, Ba substitution introduces the A-cation size variance $\sigma^2 = \langle r^2{}_A \rangle - \langle r_A \rangle^2$ as well as increasing $\langle r_A \rangle$. A convex curvature at low H/M, identified by an arrow in the $A = Sr_{0.7}Ba_{0.3}$ sample, develops as σ^2 increases; but it totally disappears in $BaRuO_3$ with $\sigma^2 = 0$. The size-variance effect is not easily distinguished in the Ca substituted samples where the structural distortion due to small $\langle r_A \rangle$ appears to contribute an overall convex curvature for isotherms in the Arrott plot. It is likely that the size variance generally causes a convex curvature at low H/M. In order to isolate the size variance effect on the curvature of isotherms, we have taken isothermal $M(H)$ curves for a series of samples $Sr_{1-z}(Ba_{0.49}Ca_{0.51})_zRuO_3$ where σ^2 increases with increasing z while $\langle r_A \rangle \approx r_{Sr}$ remains a constant for this series of samples. Increasing σ^2 reduces T_c and the saturation moment M_s(5 K) at 5 T; but more importantly, as shown in Figs. 3(a)–3(c), it converts nearly linear lines of the Arrott plot in $SrRuO_3$ into isotherms with slightly convex curvature at $H/M \approx 1000$ Oe/emu for temperatures that cross T_c.

We have also found that the curvature of isotherms in the Arrott plot depends sensitively on how the sample is made. Taking $SrRuO_3$, for example, an overall convex curvature of the isotherms in the Arrott plot is found for a polycrystalline $SrRuO_3$ sample synthesized by standard solid-state reaction at ambient pressure (AP). For a melt-grown single-crystal sample,[7] the convex curvature in the isothermal lines of the Arrott plot is clearly reduced, but it is still visible as seen in Fig. 3(e). Linear lines can be seen only in the high-pressure (HP) $SrRuO_3$ sample made under 4 GPa and at 1000 °C. Moreover, the HP sample shows $T_c \approx 167$ K and M_s(5 K) $\approx$ 1.6 μ_B/Ru at 5 T. Different procedures for the sample's preparation may lead to a subtle difference in the crystal structure. In order to demonstrate the relationship between the magnetization near T_c and crystal structure, we have made a thorough structural study on these ruthenates.

Ruthenates undergo structural transitions from the orthorhombic (*Pbnm*) phase to the orthorhombic (*Imma*) phase to the cubic (*Pm-3m*) phase as $\langle r_A \rangle$ increases. Figure 4(a) illustrates the phase diagram, which includes the evolution with $\langle r_A \rangle$ of lattice parameters in these phases. The difference of lattice parameters between AP and HP samples of $SrRuO_3$ is too small to be visualized in these phase diagrams. Because of the intrinsic structural distortion in the *Pbnm* perovskite,[11] a and b cross as $\langle r_A \rangle$ increases; a-b peaks out inside the *Pbnm* phase near the *Pbnm*/*Imma* phase boundary. The subtle change of a-b as a function of $\langle r_A \rangle$ in the *Pbnm* phase can be used to identify the difference between AP and HP samples. Figure 4(b) shows a-b versus $\langle r_A \rangle$ in a narrow range of $\langle r_A \rangle$ near A = Sr. The overall change of isotherms from a convex curvature to a concave curvature as a function of $\langle r_A \rangle$ from

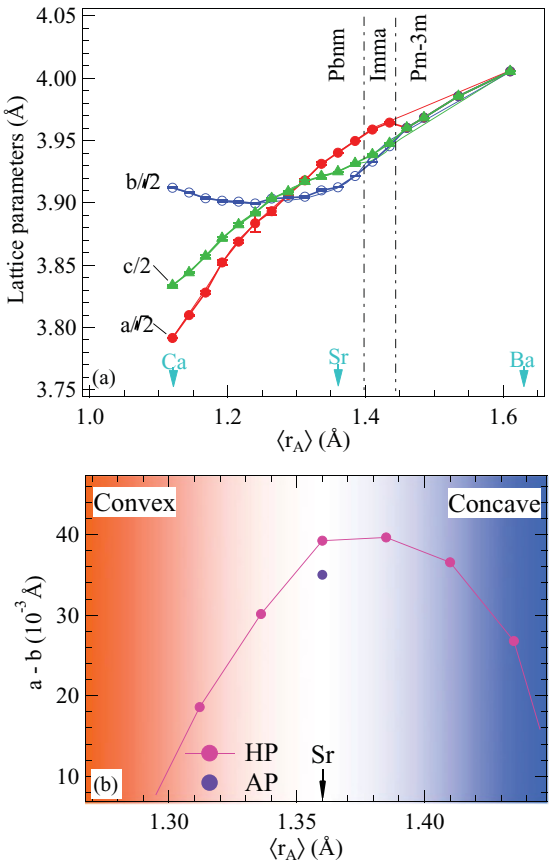

FIG. 4. (Color online) (a) Lattice parameters versus the averaged A-cation radius $\langle r_A \rangle$ in perovskite ruthenates. (b) Lattice parameters a-b versus $\langle r_A \rangle$ near $A = \mathrm{Sr}$.

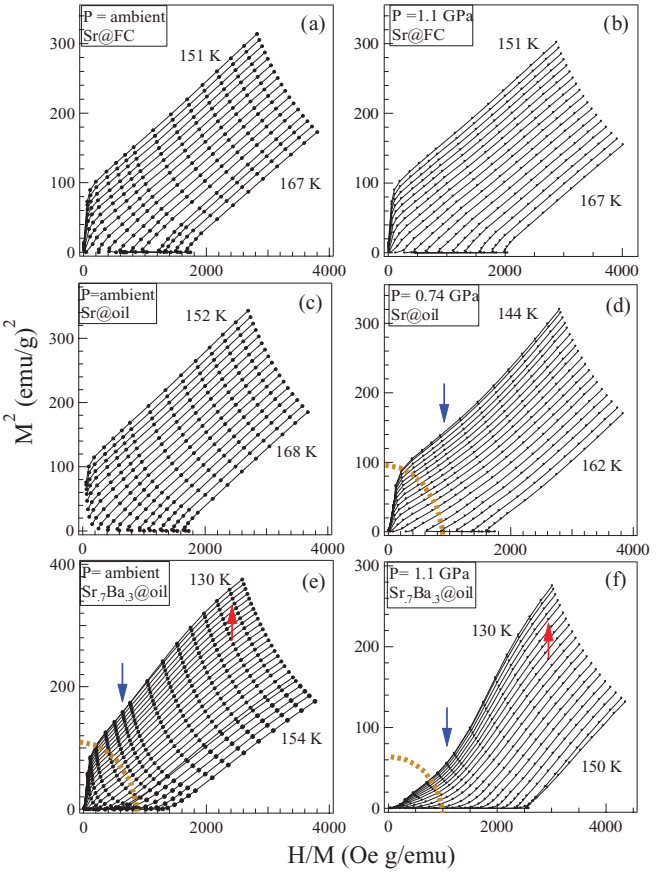

FIG. 5. (Color online) Arrott plots M^2 versus H/M for perovskites $ARuO_3$ (III. the effects of hydrostatic pressure and nonhydrostatic pressure). Panels (a) and (b) show the HP $SrRuO_3$ sample in a pressure cell filled with Fluorinert (FC). Panels (c) and (d) show the HP $SrRuO_3$ sample in a pressure cell filled with silicone oil (oil). Panels (e) and (f) show the HP $Sr_{0.7}Ba_{0.3}RuO_3$ sample in a pressure cell filled with silicone oil.

Fig. 2 are color coded in this plot. It is clear that the AP sample has smaller a-b than that in the HP sample, which makes this sample equivalent to a composition on the side of Ca-substituted samples. As a matter of fact, a-b of the single-crystal sample of Ref. 7 is also slightly smaller than that of the HP sample. Therefore, linear isotherms of an Arrott plot exist for ruthenates only within an extremely narrow range of $\langle r_A \rangle$ in the *Pbnm* phase. The HP $SrRuO_3$ just happens to fall within this range.

After demonstrating the effects of chemical substitutions on the Arrott plot, it is interesting to compare them with the pressure effect since it provides a clean tuning on the bandwidth. Depending on the property of the pressure medium, however, some nonhydrostatic pressure component, typically sheer stress, is introduced at higher pressure. Hydrostatic pressure changes the cooperative octahedral-site rotations as well as shrinking the M–O bond length in an orthorhombic perovskite AMO_3. In contrast, the shear stress due to nonhydrostatic pressure results in some local bond-length disorder. We have studied these pressure effects in two samples: the HP $SrRuO_3$ and the HP $Sr_{0.7}Ba_{0.3}RuO_3$ up to 1 GPa. The top two panels (a) and (b) in Fig. 5 show the results of the HP $SrRuO_3$ sample loaded in a high-pressure chamber filled with Fluorinert, which provides nearly hydrostatic pressure to about 1 GPa. Hydrostatic pressure does not cause any obvious changes in terms of the linear lines of the Arrott plot. In sharp contrast, nonhydrostatic pressure with silicone oil used as the pressure medium causes a clear convex curvature [indicated by an arrow in Fig. 5(d)], which is similar to the effect due to A-cation size variance in Fig. 3. Isotherms at ambient pressure of the HP $Sr_{0.7}Ba_{0.3}RuO_3$ sample measured with the high-pressure cell are displayed in Fig. 5(e); they are identical to those for the same sample measured with a straw in Fig. 2. As mentioned in the analysis of Fig. 2, complicated features of the Arrott plot in the HP $Sr_{0.7}Ba_{0.3}RuO_3$ sample are due to a combination of a convex curvature at low values of H/M due to the size-variance effect and a concave curvature at high values of H/M due to a larger $\langle r_A \rangle$ in this Ba-substituted sample. We have measured isotherms of the HP $Sr_{0.7}Ba_{0.3}RuO_3$ sample near T_c under high pressure with silicone oil used as the pressure medium. As shown in Fig. 5(f), isotherms of the sample under $P = 1.1$ GPa for the same temperature range do not have interceptions at the vertical axis, which means that T_c reduces dramatically. Moreover, a convex curvature at about $H/M = 1500$ Oe g/emu is clearly enhanced. These data suggest that disturbing the easy magnetization axis due to local structural distortions is the source of the convex curvature.

We turn to the feature of isotherms inside the dashed circle of the Arrott plot in Figs. 2, 3, and 5. Figure 6(a) is

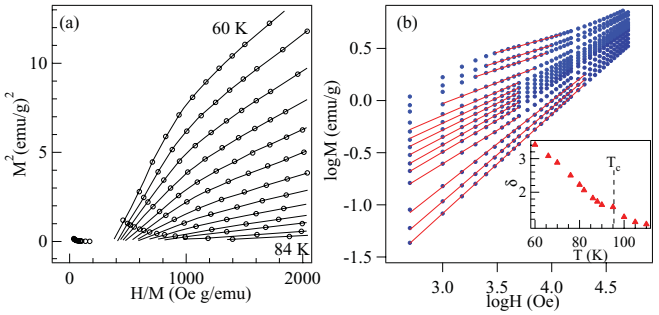

FIG. 6. (Color online) (a) A zoom-in plot of isotherms inside the dashed circle of the sample $A = Sr_{0.5}Ca_{0.5}$ in Fig. 2; (b) the log$M$ vs log$H$ plot of the same isotherms in (a). Inset is the temperature dependence of δ from the linear fitting to lines in (b).

a zoom-in plot of the panel for $A = Sr_{0.5}Ca_{.5}$ in Fig. 2. At low fields, the local structural distortion and the A-cation size variance in this sample appear to curve isotherms so that no spontaneous M_s can be resolved at $T < T_c$ and also the inverse susceptibility χ^{-1} deduced from the intercept at $M^2 = 0$ is much reduced from the intercept based on isotherms at higher H/M at $T > T_c$. These peculiar features of isotherms at low field are commonly seen in other ruthenate samples either with larger A-cation size variance in Fig. 3 or under nonhydrostatic pressure in Fig. 5. Various types of site randomness alter long-range magnetic order in Heisenberg systems. Isotherms in the Arrott plot start to experience the influence of randomness at low fields. By taking into account a random uniaxial anisotropy, Aharony and Pytte [12] predicted the behavior of isotherms at very low field for temperatures crossing T_c. Their prediction fits in principle what we have observed here. A characteristic of this type of randomness is to increase δ in $H \sim M^{\delta}$ from $\delta < 3$ ($\delta = 3$ is predicted by the mean-field theory) at T_c to $\delta > 3$ at $T < T_c$ for a three-dimensional (3D) Heisenberg system. An offset in the H/M axis for all isotherms in Fig. 6(a) is due to the demagnetization factor. Although isotherms at temperatures near $T = 60$ K cannot be fit with $H \sim M^{\delta}$ over a wide range on the H/M axis, the plot of log$M$ versus log$H$ in Fig. 6(b) and their linear fitting indeed show a continuous increase of δ in the vicinity of T_c with δ passing 3 eventually. These observations indicate that local lattice distortions and A-cation size variance result in a random uniaxial site anisotropy in the ruthenate perovskites.

In summary, the local disorders either from A-cation size variance or induced by nonhydrostatic pressure contribute complex features in an Arrott plot, which include nonparallel isotherms near the origin and a convex curvature near $H/M \sim$ 1000 Oe g/emu, as indicated by arrows in Figs. 2, 3, and 5. After clarifying the effect of local structural disorder on the magnetization, it becomes more clear that the influence from the average A-cation size $\langle r_A \rangle$ on isotherms is to change a convex curvature to a linear line to a concave curvature at higher values of H/M as $\langle r_A \rangle$ increases.

Critical exponents for the ruthenates in Fig. 2 have been obtained through iterations; an example for the HP $SrRuO_3$ sample is shown in Fig. 7. We can find at least three classes of critical behavior; namely, for a Heisenberg model ($\beta \sim 0.38$, $\gamma \sim 1.4$), for a mean-field model ($\beta \sim 0.5$, $\gamma \sim 1$), and for an

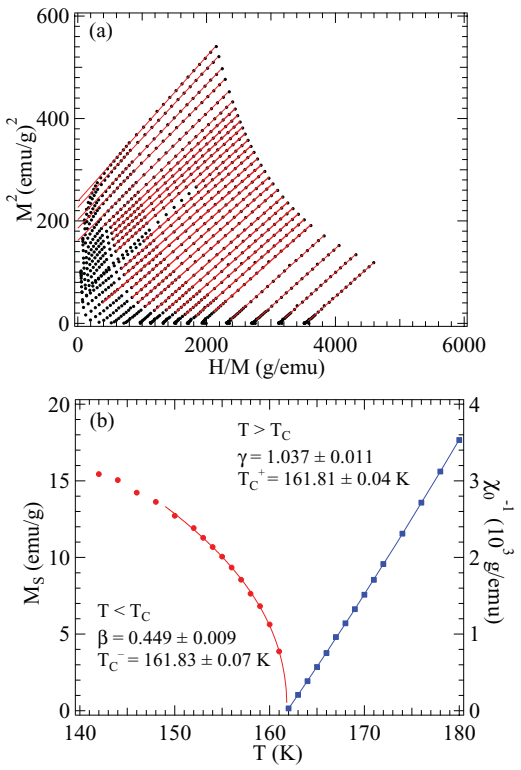

FIG. 7. (Color online) (a) Attott plot of isotherms for HP $SrRuO_3$ and their linear fittings; (b) temperature dependence of M_s and χ_0^{-1} from (a) and fitting to a power law $M_s(T) \propto |t|^{\beta}$ for $t < 0$, and $\chi_0^{-1}(T) \propto |t|^{\gamma}$ for $t > 0$; $t \equiv (T - T_c)/T_c$.

unknown universality class ($\beta > 0.5$, γ which cannot be well defined) in the plot of critical exponents versus $\langle r_A \rangle$ in Fig. 8. It is also rare that critical exponents evolve continuously between these classes. Critical-behavior analysis normally serves as a window leading to the microscopic pictures of magnetic interactions from 3D Heisenberg, XY, and Ising models to itinerant-electron ferromagnetism. Does the ruthenate system offer a case in which the fundamental magnetic interaction can be continuously tuned by the bandwidth? In order to answer this question, we look into other ferromagnetic 4d and 5d oxides; their Arrott plots are shown in Fig. 9. Although

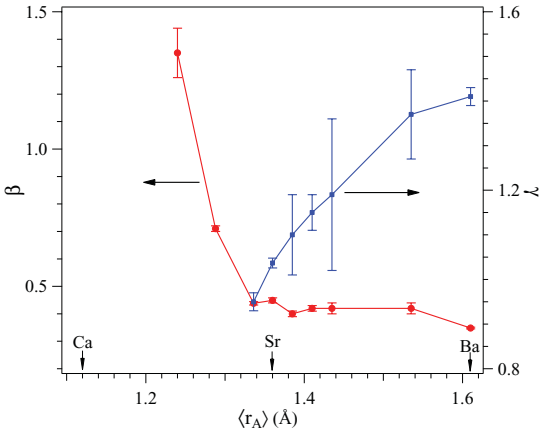

FIG. 8. (Color online) Critical exponents as a function of averaged A-cation radius in perovskite ruthenates.

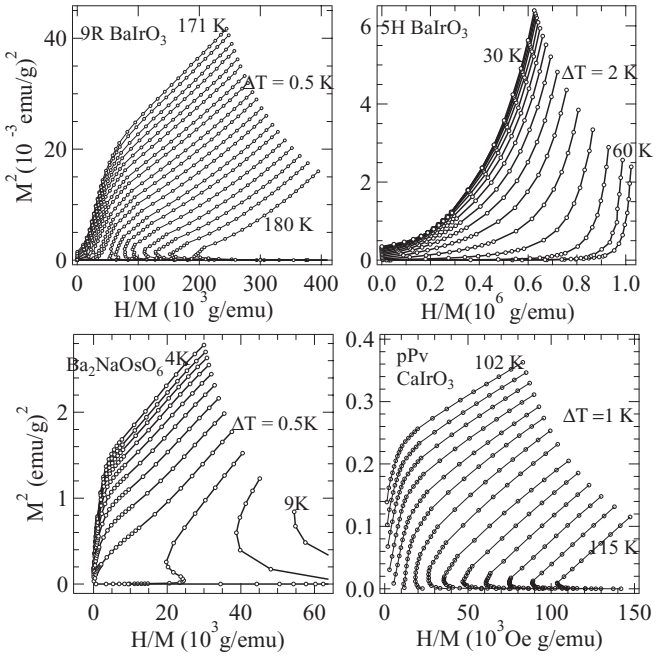

FIG. 9. Arrott plots of isotherms for four 5*d* oxide ferromagnets.

isotherms in some Arrott plots look irregular (for example, those below the charge-ordering temperature in 9R $BaIrO_3$ and above T_c in Ba_2NaOsO_6), critical-behavior analysis could be made within a very narrow temperature range near T_c. In general, curves with a convex curvature correspond to $\beta \geqslant 0.5$, which is seen in the Ca-substituted ruthenates. The mean-field model appears to be applicable to Ba_2NaOsO_6 and the postperovskite $CaIrO_3$,[13] which are insulators. These results are certainly contradictory to Stoner-Wohlfarth itinerant-electron ferromagnetism. In addition to a generally higher β found in these 5*d* metal-oxide ferromagnets than that in Heisenberg magnets, the behavior of the paramagnetic phase and how the ferromagnetic phase is approached at $T > T_c$ are also highly unusual. As shown in Fig. 10, the paramagnetic susceptibility of these 5*d* metal oxides does not follow a Curie-Weiss law. A

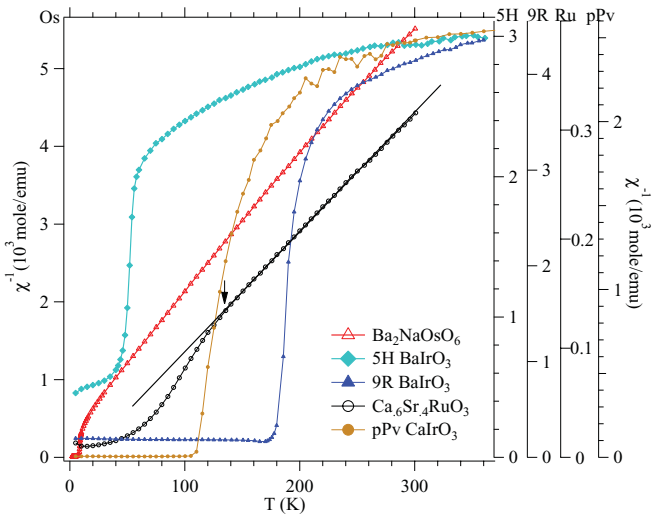

FIG. 10. (Color online) Temperature dependence of inverse magnetic susceptibility of 4*d* and 5*d* oxide ferromagnets.

T_c less than a Weiss constant is always found in a regular ferromagnet. In contrast, all Weiss constants, if they can be obtained by extrapolating from the inverse paramagnetic susceptibility above T_c, are below T_c for the ferromagnets presented in Fig. 9.

The unusual curvature and paramagnetic susceptibility are related to a strong spin-orbit coupling (SO) $\lambda \mathbf{L}\cdot\mathbf{S}$ that is on an equal footing with the spin-spin coupling in the 5*d* metal oxides. A strong SO interaction enhances both the single-ion anisotropy and the Dzyaloshinsky-Moriya interaction. The paramagnetic susceptibility of a system with a strong single-ion anisotropy energy and a Heisenberg spin-spin coupling normally does not follow a Curie-Weiss law.[14] It is interesting to make a side-by-side comparison between the Ca substituted ruthenates and these 5*d* oxide ferromagnets. Whereas the Ca-substituted samples, $Sr_{0.4}Ca_{0.6}RuO_3$, for example, share the same feature (i.e., $T_c >$ Weiss constant), the transition at T_c is much broader than that of these 5*d* oxide ferromagnets.

Narrowing the bandwidth in the Ca-substituted $Sr_{1-x}Ca_xRuO_3$ samples may lead to a phase segregation between strongly correlated and weakly correlated phases, as suggested by Rozenberg *et al.*[15] In the 4*d* and 5*d* metallic systems, an enhanced SO interaction alters the spin-spin coupling into clusters with strong correlations and clusters with $J = 0$ that dilute the ferromagnetic spin-spin interaction in the matrix. As a matter of fact, $\chi^{-1}(T)$ of $Sr_{1-x}Ca_xRuO_3$ closely resembles that typical of a Griffiths phase. The Griffiths phase is defined in the paramagnetic phase below a T_G where a $\chi^{-1}(T)$ deviates from the Curie-Weiss behavior and drops drastically as temperature lowers. The original concept was put forward by Griffith[16] to describe an Ising ferromagnetic system in which T_c is reduced due to the dilution of nonmagnetic ions. The characteristic $\chi^{-1}(T)$ of a Griffiths phase has been found in other systems than an Ising magnet.[17]

The perovskite ruthenate system is unique. The SO coupling is negligible in the end member $BaRuO_3$ with the broadest bandwidth, where a $\beta = 0.38$ typical of Heisenberg magnet is found. In the Ca-substituted $Sr_{1-x}Ca_xRuO_3$ samples, however, strong correlations result in a phase segregation into clusters with an enhanced SO coupling in a matrix of unaltered spin-spin interactions. As a result, these samples not only exhibit an unusual paramagnetic susceptibility, but also have a critical exponent $\beta \geqslant 0.5$ as found in other 5*d* metal-oxide ferromagnets. Therefore, a continuous evolution of the curvature in an Arrott plot from Ba-substituted to Ca-substituted samples implies a strengthening SO coupling as the bandwidth narrows. As in other 5*d* oxide ferromagnets, such as the postperovskite insulator $CaIrO_3$, observation of mean-field exponents $\beta \approx 0.5$ and $\gamma \approx 1$ in $SrRuO_3$ is part of a curvature evolution of the Arrott plot as a result of increasing spin-orbit coupling in a narrow-band ferromagnet and does not signal Stoner-Wohlfarth ferromagnetism.

Moreover, the fact that the ferromagnetic phase in $BaRuO_3$ collapses abruptly to a Pauli paramagnetism at a $P_c < 8$ GPa[10] and that a localized low-spin Ru(IV) configuration could have a total quantum number $J = 0$ in nonmagnetic clusters of a Griffiths phase in the Ca-substituted $Sr_{1-x}Ca_xRuO_3$ samples provide evidence that the strong ferromagnetism of $ARuO_3$ perovskites is a distinct phase appearing at the crossover from weakly correlated itinerant to localized Ru 4*d* electrons. The system provides a clear example of how the spin-orbit coupling

of a narrow-band system increases with band narrowing until it induces a transition to localized-electron behavior.

IV. CONCLUSION

The magnetizations as presented in an Arrott plot in the perovskite ruthenates has been thoroughly investigated. Results from this study include effects on an Arrott plot of the bandwidth, the size variance, and hydrostatic pressure versus nonhydrostatic pressure. At low H/M, isotherms in an Arrott plot are very sensitive to local site disorder either from A-site size variance or induced by nonhydrostatic pressure. However, the curvature of isotherms at higher H/M depends only on the bandwidth. It has been found that the convex curvature is correlated with the unusual paramagnetic susceptibility in the Ca-substituted samples and other 5d metal-oxide ferromagnets in which a spin-orbit coupling is strong. The overall curvature change from the concave curvature in $BaRuO_3$ to linear lines in $SrRuO_3$ to convex curvature in Ca-substituted $Sr_{1-x}Ca_xRuO_3$ reflects a progressive strengthening of a spin-orbit coupling as the Ru 4d bandwidth narrows in a distinct strong-ferromagnet phase appearing between a weakly correlated itinerant-electron phase and a localized-electron phase. Since the curvature in the Arrott plot of the magnetization in ruthenates is highly sensitive to structural distortions due to the chemical substitution on the A site, the critical analysis based on the Arrott plot becomes unreliable for the entire perovskite family of $ARuO_3$. Neither the linear Arrott plot in $SrRuO_3$ nor a Heisenberg behavior in a modified Arrott plot for $BaRuO_3$ truly reflects the fundamental magnetic coupling. Other thermodynamic measurements are needed in order to clarify this issue.

ACKNOWLEDGMENTS

This work was supported by Robert A. Welch foundation and the NSF (DMR 0904282, 1122603) in the US and MOST in China. J. S. Z. is grateful to F. Rivadulla for informing us about Ref. 12.

*jszhou@mail.utexas.edu

[1] A. Arrott and J. E. Noakes, Phys. Rev. Lett. **19**, 786 (1967).
[2] E. P. Wohlfarth, J. Appl. Phys. **39**, 1061 (1968).
[3] H. E. Stanley, *Introduction to Phase Transition and Critical Phenomena* (Oxford University Press, New York, 1971).
[4] T. Moriya, *Spin Fluctuations in Itinerant Electron Magnetism* (Springer-Verlag, Berlin, 1985).
[5] G. G. Lonzarich and L. Taillefer, J. Phys. C **18**, 4339 (1985).
[6] Y. Takahashi, J. Phys. Soc. Jpn. **55**, 3553 (1986).
[7] D. Kim, B. L. Zink, F. Hellman, S. McCall, G. Cao, and J. E. Crow, Phys. Rev. B **67**, 100406(R) (2003).
[8] K. Yoshimura, T. Imai, T. Kiyama, K. R. Thurber, A. W. Hunt, and K. Kosuge, Phys. Rev. Lett. **83**, 4397 (1999).
[9] Jing Xia, W. Siemons, G. Koster, M. R. Beasley, and A. Kapitulnik, Phys. Rev. B **79**, 140407 (2009).
[10] J.-S. Zhou, K. Matsubayashi, Y. Uwatoko, C.-Q. Jin, J.-G. Cheng, J. B. Goodenough, Q. Q. Liu, T. Katsura, A. Shatskiy, and E. Ito, Phys. Rev. Lett. **101**, 077206 (2008).
[11] J.-S. Zhou and J. B. Goodenough, Phys. Rev. Lett. **94**, 065501 (2005).
[12] A. Aharony and E. Pytte, Phys. Rev. Lett. **45**, 1583 (1980).
[13] J.-G. Cheng, J.-S. Zhou, J. B. Goodenough, Y. Sui, Y. Ren, and M. R. Suchomel, Phys. Rev. B **83**, 064401 (2011).
[14] J. Kanamori, Prog. Theor. Phys. **17**, 177 (1957).
[15] M. J. Rozenberg, G. Kotliar, and X. Y. Zhang, Phys. Rev. B **49**, 10181 (1994).
[16] R. B. Griffiths, Phys. Rev. Lett. **23**, 17 (1969).
[17] M. B. Salamon, P. Lin, and S. H. Chun, Phys. Rev. Lett. **88**, 197203 (2002).